

Article

Evolution of the Electronic Structure of the *trans*-[Re₆S₈bipy₄Cl₂] Octahedral Rhenium Cluster during Reduction

 Maxim R. Ryzhikov , Yakov M. Gayfulin , Anton A. Ulantikov, Dmitry O. Arentov, Svetlana G. Kozlova  and Yuri V. Mironov 

Nikolaev Institute of Inorganic Chemistry SB RAS, 3, Acad. Lavrentiev Ave., 630090 Novosibirsk, Russia

* Correspondence: maximato@mail.ru (M.R.R.); yuri@niic.nsc.ru (Y.V.M.)

Abstract: Understanding the processes that occur during the redox transformations of complexes coordinated by redox-active apical ligands is important for the design of electrochemically active compounds with functional properties. In this work, a detailed analysis of the interaction energy and electronic structure was performed for cluster complexes *trans*-[Re₆S₈bipy₄Cl₂]ⁿ (n = 2−, 4−, 6−, 8−), which can be obtained by stepwise electrochemical reduction of a neutral cluster *trans*-[Re₆S₈bipy₄Cl₂] in DMSO solution. It was shown that the formation of open-shell paramagnetic ions with S = 1, 2 and 1 is the most energetically favorable for n = 2−, 4− and 6−, respectively.

Keywords: octahedral rhenium clusters; reduction; DFT; ELF; cyclic voltammetry



Citation: Ryzhikov, M.R.; Gayfulin, Y.M.; Ulantikov, A.A.; Arentov, D.O.; Kozlova, S.G.; Mironov, Y.V. Evolution of the Electronic Structure of the *trans*-[Re₆S₈bipy₄Cl₂] Octahedral Rhenium Cluster during Reduction. *Molecules* **2023**, *28*, 3658. <https://doi.org/10.3390/molecules28093658>

Academic Editor: Oleg V. Mikhailov

Received: 30 March 2023

Revised: 19 April 2023

Accepted: 21 April 2023

Published: 23 April 2023



Copyright: © 2023 by the authors. Licensee MDPI, Basel, Switzerland. This article is an open access article distributed under the terms and conditions of the Creative Commons Attribution (CC BY) license (<https://creativecommons.org/licenses/by/4.0/>).

1. Introduction

The design of electrochemically active complexes of transition metals has been a frontier area of inorganic chemistry in recent decades. Interest in the preparation of such complexes is caused by their potential for use as materials for electrocatalysis and photocatalysis, optical applications, and the preparation of redox-active coordination polymers and compounds with cooperative magnetic effects [1–4]. The study of soluble molecular redox-active compounds as electronic reservoirs and charge carriers in chemical current sources has also become an important area of research [5]. Existing approaches to the design of redox-active compounds in most cases include the preparation of mononuclear or polynuclear transition metal complexes with redox-active (non-innocent) ligands [6–9]. This strategy makes it possible to obtain complexes capable of multi stage oxidation and reduction in a wide range of applications. In these processes, many effects arise that are interesting for research from a fundamental point of view. Such effects, in particular, are the mutual influence of the metal cation and the ligand on the electronic structure and the spectroscopic properties and stability of the oxidized and reduced forms of the complexes.

In the past few years, a great amount of attention has been attracted to redox-active transition metal cluster compounds and, in particular, octahedral clusters of {M₆Q₈} type [10–15]. These complexes are based on an octahedral core consisting of six metal cations linked to each other by covalent bonds. The metal core is coordinated by a set of eight “inner” ligands lying on the faces of the octahedron, and six apical ligands, one for each metal atom. As a result, the general formula for these cluster complexes can be written as [{M₆Q₈}L₆]ⁿ, where Q and L denote inner and apical ligands, respectively. The presence of covalent bonds in the cluster core leads to a unique electronic structure where the atomic orbitals of the metal atoms and inner ligands overlap and form a set of frontier orbitals, which are delocalized over all atoms of the cluster core [10]. Therefore, the cluster core can be considered a single metal ion coordinated by a set of apical ligands.

Cluster cores {M₆Q₈} are capable of oxidation, which is associated with a decrease in the number of electrons localized in bonding metal-centered molecular orbitals (cluster skeletal

electrons, CSE). The effects of coordination of various N-donor [16–19], P-donor [20–22], and O-donor [23–26] apical ligands on the potentials of these oxidative transitions have been studied in detail. On the other hand, attempts to reduce the $\{M_6Q_8\}$ cluster cores to 25 CSE led to irreversible processes associated with the destruction of the cluster core due to the strongly antibonding character of the lowest metal-centered unoccupied orbitals. However, as in the case of single metal ions, the coordination of redox-active (non-innocent) apical ligands to the cluster cores often makes it possible to obtain compounds capable of reversible reduction due to the presence of low-lying ligand-centered π^* molecular orbitals. For example, $\{Mo_3S_4\}$ clusters decorated with redox active diimine ligands demonstrate multistage reduction processes [27–29]. It was also shown that the coordination of pyridine derivatives to $\{Re_6Q_8\}$ cluster cores often led to the obtaining of compounds exhibiting multielectron reduction processes in cyclic voltammograms [16,19]. All these clusters can act as multi electron reservoirs, which may allow them to be used in catalytic and magnetochemical applications.

In recent years, we have synthesized and investigated a series of new redox-active octahedral rhenium cluster complexes coordinated by redox-active N-donor ligands. Particularly, molecular clusters with the general formula *trans*- $[Re_6Q_8L_4X_2]$ ($Q = S$ or Se , $X = Cl^-$, Br^- or CN^-) were obtained for $L = 4,4'$ -bipyridine, 4-phenylpyridine, *trans*-1,2-Bis(4-pyridyl)ethylene, and 1,3-Bis(4-pyridyl)propane [30–33]. Electrochemical investigation of the compounds *trans*- $[Re_6Q_8bipy_4X_2]$ ($Q = S$ or Se ; $X = Cl$ or Br ; $bipy = 4,4'$ -bipyridine) (Figure 1) showed that the complexes are capable of accepting up to eight electrons per ligand-centered molecular orbitals, each localized to two bipy molecules in the *trans*-position [30]. In this case, the chemical preparation of the reduced forms was difficult due to the low solubility of the compounds and the low potentials required. However, since the reduction of free 4,4'-bipyridine leads to the production of radical anions, the reduction of compounds *trans*- $[Re_6Q_8bipy_4X_2]$ can potentially lead to the formation of paramagnetic radical anions with up to four unpaired electrons. The possibility of obtaining such polyradicals can stimulate further research in this area; therefore, the aim of this article was to determine the preferable electron configuration of $[Re_6S_8bipy_4Cl_2]^n$ clusters, with $n = 0, 2-, 4-, 6-, 8-$, by DFT calculations and to trace changes in the electronic structure during reduction.

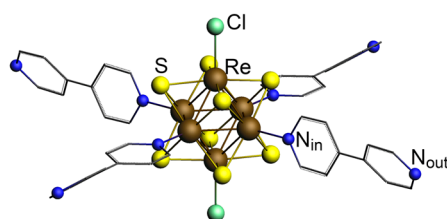


Figure 1. The structure of the *trans*- $[Re_6S_8bipy_4Cl_2]$ cluster. The hydrogen atoms of bipyridine ligands are removed for clarity.

2. Computational Details

The geometry optimization and frequency calculations of the $[Re_6S_8bipy_4Cl_2]^n$ clusters in $n = 0, 2-, 4-, 6-, 8-$ oxidation states were performed in the ADF2017 [34,35] program suite with generalized gradient approximation (GGA) dispersion corrected S12g [36] density functional, all-electron STO's TZP [37] basis set, and zero-order regular approximation (ZORA) [38] to take into account scalar relativistic effects. Since dimethyl sulfoxide (DMSO) was previously used for electrochemical investigations of the $[Re_6S_8bipy_4Cl_2]^0$ cluster [30], it was used as the solvent for calculations. The conductor-like screening model (COSMO) [39] was used to take into account the DMSO environment. The spin-restricted ($S = 0$) approximation was used for the cluster in all oxidation states. The spin-unrestricted approximation was additionally used for 2- ($S = 1$), 4- ($S = 1$ and $S = 2$), and 6- ($S = 1$) oxidation states. Since the $[Re_6S_8bipy_4Cl_2]^n$ clusters are characterized by eight pyridine heterocycles that could be difficult to optimize in internal coordinates, the Cartesian coordinate space was used for geometry optimization. The optimization process started with the

C_i symmetry as it was found in the crystal structure of the neutral $[\text{Re}_6\text{S}_8\text{bipy}_4\text{Cl}_2]^0$ cluster. However, some of the structures optimized at C_i symmetry have imaginary frequencies (typically with $S = 0$ spin state). In such a case, the symmetry was lowered to C_1 . Thus, it was possible to achieve structures without imaginary frequencies. Note that most of the structures optimized at C_1 symmetry ($n = 2-, S = 0$; $n = 6-, S = 0$; $n = 6-, S = 1$ and $n = 8-, S = 0$) are still close to the C_i symmetry, with the root mean square (RMS) deviation from C_i not exceeding 0.04 \AA . The only exception is the $[\text{Re}_6\text{S}_8\text{bipy}_4\text{Cl}_2]^{4-} S = 0$ cluster with a structure closer to C_2 (still quite far RMS 0.07 \AA). The geometry optimization calculations performed at the S12g/TZP level of theory typically gives good structural parameters for transition metal compounds in a reasonable amount of time [40–43]. The optimized coordinates of the $[\text{Re}_6\text{S}_8\text{Cl}_2\text{bipy}_4]^n$ cluster in all oxidation and spin states are summarized in Tables S1–S9.

Since GGA functionals typically underestimate the gap between occupied and unoccupied levels, single-point calculations with the S12h [35] dispersion-corrected hybrid density functional, all-electron TZ2P basis set, COSMO model for the DMSO environment, and scalar relativistic ZORA were performed on optimized geometries. The calculation and analysis of the electron localization function (ELF) [44,45] were performed in the dgrid-4.6 [46] program with a 0.05 a.u. mesh step. The atomic charges were calculated by the definition of the quantum theory of atoms in molecules (QTAIM) [47]. In the QTAIM, the atomic basin is defined as all points of the space in which the gradient line finishes in the atomic attractor (the local maximum of electron density located at the position of the atom nucleus). To obtain the atomic charges within QTAIM, the electron density must be integrated over the volume of the corresponding basin. The QTAIM charges were calculated with the built-in ADF tools with default settings. Since the integration is performed numerically over real space, an error could arise for heavy atoms, which have a strong nonlinearity of the electron density near the nucleus. The deviations of the total number of electrons after integration from the necessary value do not exceed $0.0008 e$, indicating good integration grid accuracy.

The energy decomposition analysis (EDA) [48] calculations were performed in ADF2020 [49] to analyze the interaction energy (E_{int}) between $\text{Re}_6\text{S}_8\text{Cl}_2$ and $[\text{bipy}_4]^n$ fragments at the same theoretical level as single-point calculations. In all EDA calculations, the $\text{Re}_6\text{S}_8\text{Cl}_2$ cluster fragment was taken as neutral and spin-restricted, while the charge and the spin state of the $[\text{bipy}_4]^n$ fragment were taken in accordance with the respective properties of the whole cluster $[\text{Re}_6\text{S}_8\text{Cl}_2\text{bipy}_4]^n$.

3. Results and Discussion

It was shown that the reduction of the $[\text{Re}_6\text{S}_8\text{bipy}_4\text{Cl}_2]^n$ cluster occurs in four waves in cyclic voltammetry (CV) experiments, and each wave corresponds to the transfer of approximately two electrons [30]. Therefore, the cluster was calculated with $n = 0, 2-, 4-, 6-$ and $8-$. The unoccupied frontier molecular orbitals (Figure 2) of the neutral $[\text{Re}_6\text{S}_8\text{bipy}_4\text{Cl}_2]^0$ cluster are almost degenerate ($E_{\text{LUMO}+1} - \text{LUMO} = 0.021 \text{ eV}$ and $E_{\text{LUMO}+3} - \text{LUMO}+2 = 0.005 \text{ eV}$ at S12h/TZ2P//S12g/TZP level of theory). Thus, the reduced states may have an open-shell electronic structure. The comparison of the relative energies (Table 1) shows that the most stable spin states are 1, 2, and 1 for the cluster in $2-, 4-,$ and $6-$ oxidation states, respectively. The cluster in ($n = 0; S = 0$), ($n = 2-; S = 1$), ($n = 4-; S = 2$), ($n = 6-; S = 1$), and ($n = 8-; S = 0$) oxidation and spin states will be used for subsequent study.

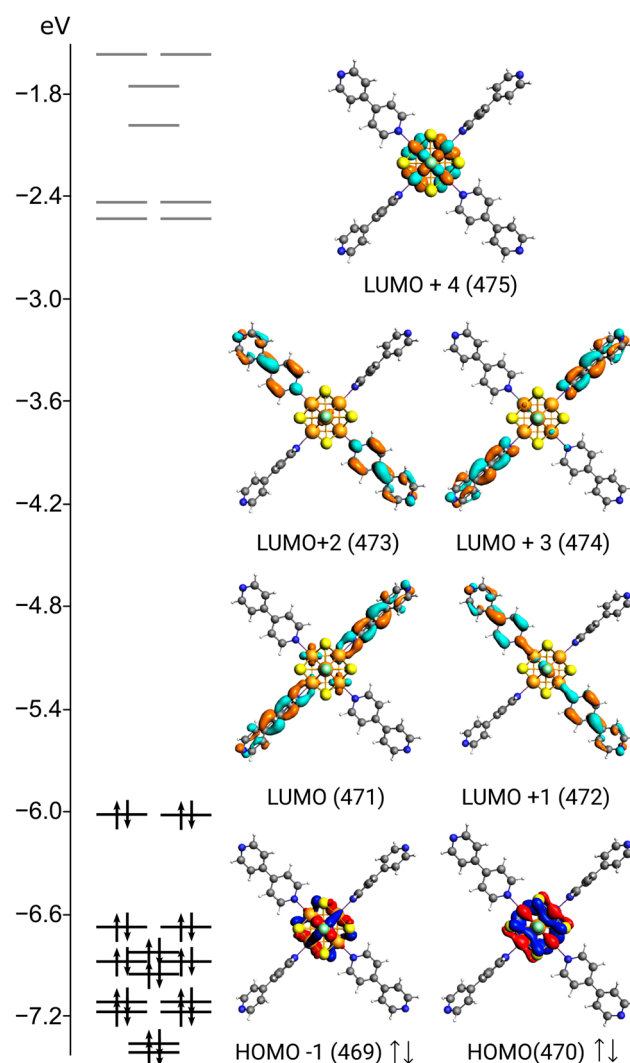


Figure 2. The diagram of the energy levels and isosurfaces of the MOs for the $[\text{Re}_6\text{S}_8\text{bipy}_4\text{Cl}_2]^0$ cluster.

Table 1. Average interatomic distances (Å) and relative energies (eV) for $[\text{Re}_6\text{S}_8\text{bipy}_4\text{Cl}_2]^n$ clusters in different oxidation (n) and spin (S) states.

n	0	2−		4−			6−		8−
S	0	0	1	0	1	2	0	1	0
$\langle d(\text{Re-Re}) \rangle$	2.61	2.61	2.61	2.62	2.62	2.61	2.62	2.62	2.62
$\langle d(\text{Re-Cl}) \rangle$	2.44	2.46	2.46	2.48	2.49	2.48	2.51	2.51	2.55
$\langle d(\text{Re-S}) \rangle$	2.42	2.42	2.42	2.42	2.42	2.42	2.42	2.42	2.43
$\langle d(\text{Re-N}_{\text{in}}) \rangle$	2.21	2.17	2.17	2.14	2.14	2.15	2.12	2.12	2.11
$\Delta E(\text{S12g/TZP})$	0.00	−6.24	−6.32	−11.95	−12.07	−12.16	−16.93	−16.99	−21.22
$\Delta E(\text{S12h/TZ2P//S12g/TZP})$	0.00	−5.25	−5.54	−10.45	−11.12	−11.76	−15.51	−15.87	−20.42

Four redox transitions in CV allow the comparison of the experimental half-wave potential ($E_{1/2}^1$) values [30] with relative energies (ΔE) of the cluster in different oxidation states (Figure 3). The experimental and calculated points can be fitted by a straight line with 0.993 and 0.995 R^2 values for S12g/TZP and S12h/TZ2P//S12g/TZP levels of theory, respectively. Such R^2 values indicate that the electronic structure changes occurring in the

cluster during electrochemical reduction can be reproduced with a good accuracy at both theoretical levels.

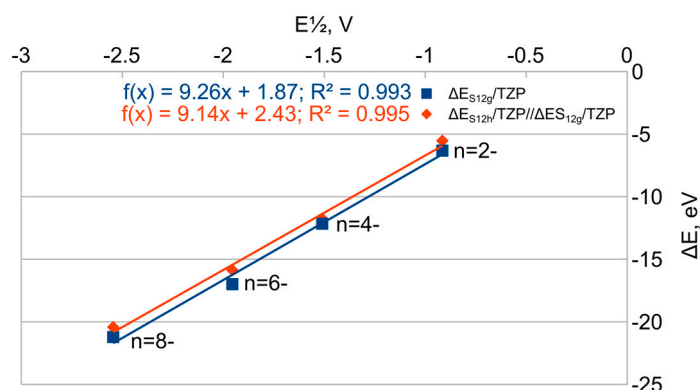


Figure 3. $E_{1/2}$ (V) vs. ΔE (eV) plot for S12g/TZP (◆) and S12h/TZ2P//S12g/TZP (■) levels of theory.

The formation of the four lowest unoccupied molecular orbitals of the neutral $[\text{Re}_6\text{S}_8\text{bipy}_4\text{Cl}_2]^0$ cluster can be traced starting from the LUMO orbital of individual bipy ligands, through the model fragment of four bipy ligands to the complete cluster (Figure 4). As can be seen, the LUMO of the two bipy molecules in *trans*-positions solely forms the LUMO, LUMO + 1, LUMO + 2, and LUMO + 3 of the bipy_4 fragment. These MOs are composed of bipy's LUMO with an almost equal contribution, making them very close in energy ($\Delta E = 0.01$ eV). It is clear that the pairing of bipy's LUMO in *trans*-positions is explained by the number of possible combinations. Four LUMOs of bipy in *trans*-positions can form the four MOs (two bonding and two antibonding) (Figure 4), while four LUMOs of bipy in *cis*-positions can form eight MOs (four bonding and four antibonding) (Figure S1), which did not correlate with the number of original states (four LUMO of bipy). The addition of the $\text{Re}_6\text{S}_8\text{Cl}_2$ cluster fragment to the bipy_4 fragment slightly changes the order of the four lowest unoccupied MOs. However, the four lowest unoccupied orbitals of the $[\text{Re}_6\text{S}_8\text{bipy}_4\text{Cl}_2]^0$ cluster are still composed mainly of the orbitals of the bipy_4 fragment.

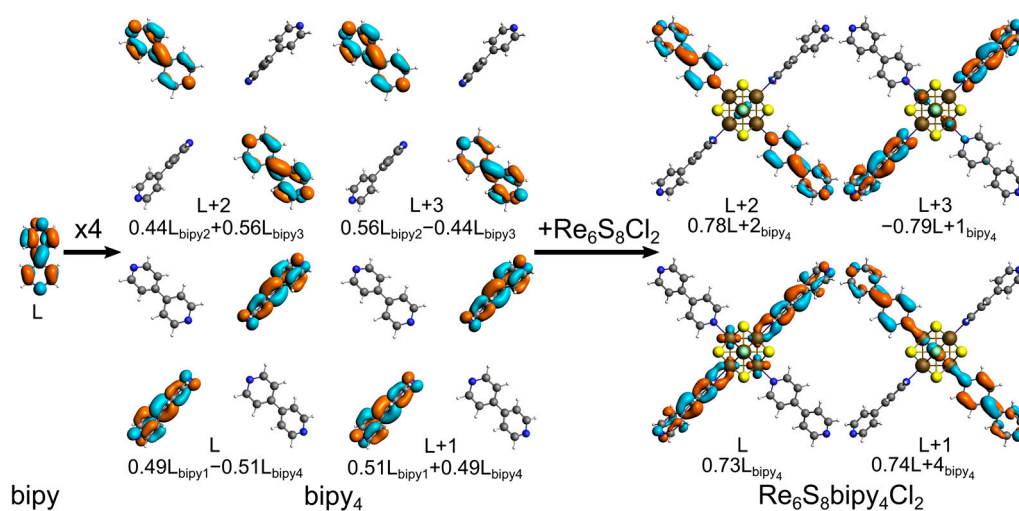


Figure 4. Schematic representation of the four lowest unoccupied orbitals formation starting from the LUMO of the bipy, through the LUMO, LUMO + 1, LUMO + 2, and LUMO + 3 orbitals of the bipy_4 fragment, to the LUMO, LUMO + 1, LUMO + 2, and LUMO + 3 orbitals of the $[\text{Re}_6\text{S}_8\text{bipy}_4\text{Cl}_2]^0$ cluster.

The interatomic distances in the cluster core ($d(\text{Re}-\text{Re})$ and $d(\text{Re}-\text{S})$) of the $[\text{Re}_6\text{S}_8\text{bipy}_4\text{Cl}_2]^n$ clusters are almost constant during the reduction process (Table 1). The distances between rhenium atoms and the atoms of the terminal ligands are more sensitive to the reduction. The unoccupied orbitals of the neutral $[\text{Re}_6\text{S}_8\text{bipy}_4\text{Cl}_2]^0$ cluster, which is populated during reduction

(LUMO, LUMO + 1, LUMO + 2 and LUMO + 3), are primary localized on the bipy ligands. However, the Re–Cl distances become 0.9 Å longer for eight-electron reduction, indicating significant bond weakening (Table 1). In contrast, the Re–N_{in} bonds display a large shortening from 2.21 Å to 2.12 Å during reduction of the cluster, which correlates with the contribution of the bonding Re–N_{in} interaction in the four lowest unoccupied MOs (Figure 4).

Based on the calculated energies (Table 1) and the molecular orbitals (Figure 5) of the cluster with the different charges, the following process of reduction can be proposed. The pair of molecular orbitals delocalized over bipy ligands in trans position are occupied by a single electron each during the first two-electron reduction wave, and the resulting $[\text{Re}_6\text{S}_8\text{bipy}_4\text{Cl}_2]^{2-}$ cluster has two unpaired electrons. The second two-electron reduction wave leads to the occupation of the two additional MOs by a single electron each, with the formation of the $[\text{Re}_6\text{S}_8\text{bipy}_4\text{Cl}_2]^{4-}$ cluster with four unpaired electrons. In this case, all four of the bipy₄-centered orbitals become populated by a single electron each. During the consequent reduction wave, two orbitals already populated by the single electron are occupied by two additional electrons, reducing the number of unpaired electrons to two in the $[\text{Re}_6\text{S}_8\text{bipy}_4\text{Cl}_2]^{6-}$ cluster. The final wave causes all four orbitals to become populated by two electrons each in the $[\text{Re}_6\text{S}_8\text{bipy}_4\text{Cl}_2]^{8-}$ cluster. Thus, the four bipy₄-centered orbitals can roughly be considered as a separate electronic shell that populates according to Hund's rule. Finally, the eight-electron reduction by the four two-electron reduction waves is shown in Scheme 1.

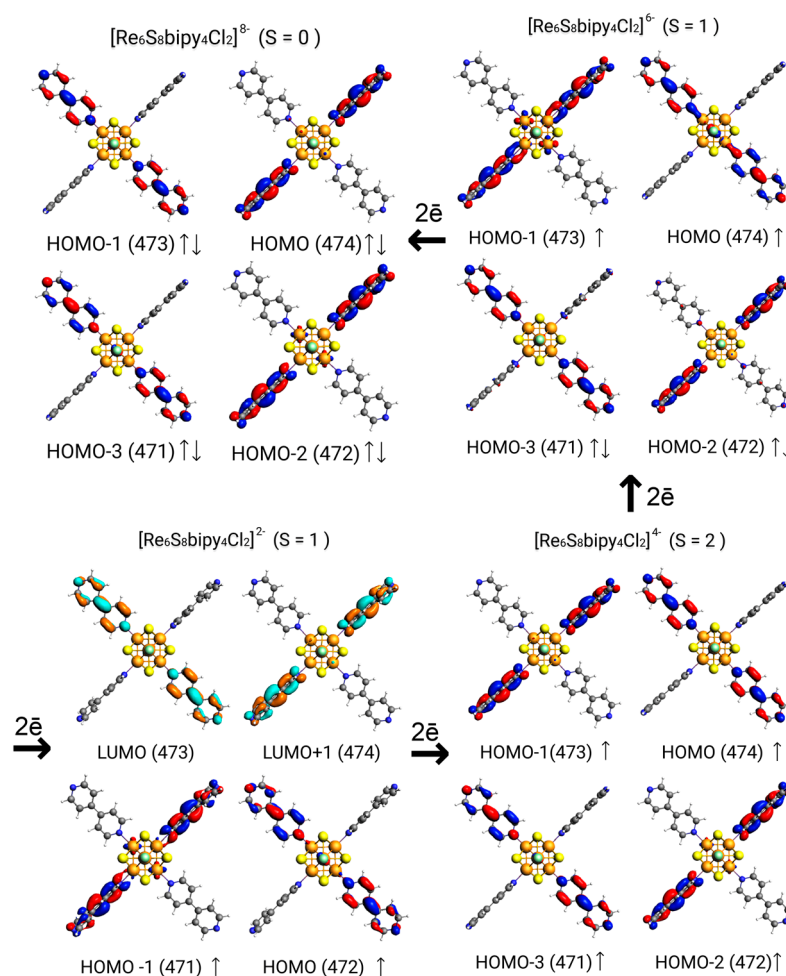
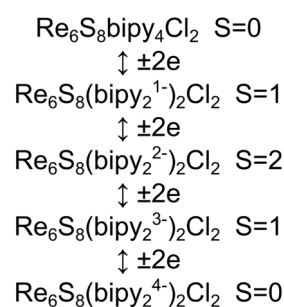


Figure 5. Occupation of the frontier orbitals during the reduction of the $[\text{Re}_6\text{S}_8\text{bipy}_4\text{Cl}_2]^n$ clusters.



Scheme 1. Changes in the charges and spin states during eight-electron reduction of the $[\text{Re}_6\text{S}_8\text{bipy}_4\text{Cl}_2]^0$ cluster.

Since the MOs in the $[\text{Re}_6\text{S}_8\text{bipy}_4\text{Cl}_2]^0$ cluster are delocalized over a large number of atoms, changes in bonding during the reductions are difficult to trace by the MO analysis. ELF analysis was used to reveal changes in bonding, as it was shown to give good results for other cluster compounds [50]. The ELF basin pattern in the $\{\text{Re}_6\}$ cluster core is quite stable during the eight-electron reduction (Table 2). In all oxidation states, there are 12 disynaptic $V(\text{Re},\text{Re})$ basins with an average population of 0.53–0.54 e and eight trisynaptic $V(\text{Re}_3)$ basins with an average population of 0.16 e. The $V(\text{Re},\text{Re})$ and $V(\text{Re}_3)$ basins indicate the two-center and three-center covalent interactions, respectively. At some oxidation states, there are also polysynaptic $V(\text{Re}_6)$ and $V(\text{Re}_5)$ basins, but the populations of such basins are negligible. The most pronounced changes are found for $V(\text{Re},\text{N}_{\text{in}})$ basins (Figure S2), in which populations grow from 2.59 e in the neutral cluster to 3.45 e in the octa-charged anionic cluster. Note that the charges on the N_{in} and Re atoms did not change substantially (Table S10). The population of $V(\text{N}_{\text{in}},\text{C})$ basins decreases from 2.42 to 2.01 e during reduction due to the antibonding nature of LUMO, LUMO+1, LUMO+2, and LUMO+3 relative to the $\text{N}_{\text{in}}\text{--C}$ interactions. Thus, four $V(\text{Re},\text{N}_{\text{in}})$ basins in total took ~ 3.5 additional electrons due to the redistribution of electron density from $V(\text{N}_{\text{in}},\text{C})$ basins, during eight-electron reduction. As was previously shown [51], the population of the basins could reflect the strength of interactions between fragments. Thus, the interaction energy between the $\text{Re}_6\text{S}_8\text{Cl}_2$ cluster fragment and the $[\text{bipy}_4]^n$ ligand fragment in different oxidation states ($n = 0, 2-, 4-, 6-$ and $8-$) was calculated and compared with the population of the $V(\text{Re},\text{N}_{\text{in}})$ basins. The linear dependency between the interaction energy (E_{int}) of the fragments and the $V(\text{Re},\text{N}_{\text{in}})$ basin population was obtained (Figure 6) with good accuracy ($R^2 = 0.98$). The fitting line crosses the x axis at a non-zero value, indicating that a population of ~ 1.0 e must be present on the $V(\text{Re},\text{N}_{\text{in}})$ basins to compensate the repulsion between the fragments. A similar result was previously obtained for a heterometallic cubane-type cluster [51].

Table 2. The average populations of the selected ELF basins for $[\text{Re}_6\text{S}_8\text{bipy}_4\text{Cl}_2]^n$ clusters in different oxidation states (n) and spin states (S).

	n = 0 S = 0	n = 2- S = 1	n = 4- S = 2	n = 6- S = 1	n = 8- S = 0
$V(\text{Re},\text{Re})$	0.54	0.53	0.54	0.53	0.54
$V(\text{Re}_3)$	0.16	0.16	0.16	0.16	0.16
$V(\text{Re}_6)$	0.01	0.03	-	-	-
$V(\text{Re}_5)$	-	-	0.01	0.01	-
$V(\text{Re},\text{N}_{\text{in}})$	2.59	2.80	3.05	3.21	3.45
$V(\text{N}_{\text{out}})$	2.76	2.85	2.99	3.12	3.32
$V(\text{N}_{\text{in}},\text{C})$	2.42	2.31	2.18	2.11	2.01
$V(\text{Re},\text{Cl})$	1.11	1.14	1.14	1.16	1.15

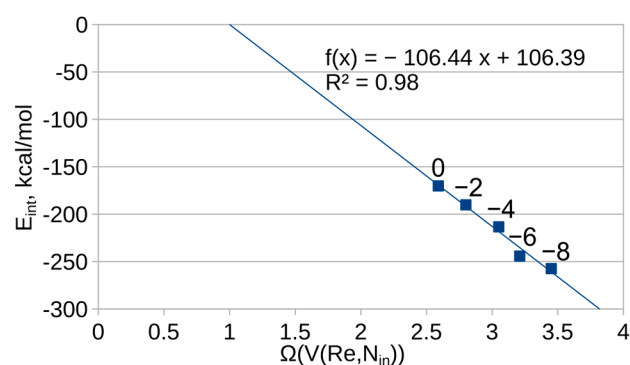


Figure 6. The relationship between $V(\text{Re}, N_{\text{in}})$ basin populations and the interaction energies (E_{int}) between $\text{Re}_6\text{S}_8\text{Cl}_2$ and $[\text{bipy}_4]^n$ fragments in the $[\text{Re}_6\text{S}_8\text{Cl}_2\text{bipy}_4]^n$ ($n = 0, 2-, 4-, 6-$ and $8-$) clusters.

4. Conclusions

Octahedral cluster complexes of rhenium with electrochemically inactive ligands are incapable of reversible reduction due to the instability of the cluster core when filling metal-centered antibonding unoccupied orbitals. The ability to reversible reduction associated with the filling of π^* orbitals of coordinated 4,4'-bipyridine molecules is the key feature of the *trans*- $[\text{Re}_6\text{S}_8]\text{bipy}_4\text{Cl}_2$ cluster complex. The aim of this study was to determine which charge states of the reduced *trans*- $[\text{Re}_6\text{S}_8]\text{bipy}_4\text{Cl}_2]^{n-}$ are energetically most preferable and how the electronic structure of the cluster changes during reduction. Analysis of the formation energies has shown that the intermediate oxidation states ($n = 2-, 4-, 6-$) of the cluster are more stable in the open-shell configuration, indicating the paramagnetic nature of the reduced species. Such behavior can be explained by the nature of the four lowest unoccupied orbitals of the neutral cluster. Since the four lowest orbitals are delocalized mainly on bipy ligands in *trans*-positions, their energies are very close to each other; thus, the orbitals are almost degenerate and filled according to Hund's rule. A notable decrease in the Re–N distances upon reduction indicates the enhancement of the bonding between the cluster core and bipy ligands upon reduction, which was confirmed by EDA. The opposite effect was found for Re–Cl bonds. The reduction of these clusters has practically no effect on the bond lengths inside the $[\text{Re}_6\text{S}_8]$ cluster core, which indicates the absence of its destabilization when electrons are localized on apical redox-active ligands. It was also shown that the interaction energy between the cluster core and bipy ligands correlates linearly with the population of the $V(\text{Re}, N_{\text{in}})$ ELF basin. The behavior, when the basin population correlates with some bond related properties, is intuitive but does not have much confirmation in the literature [51–53]. Finally, since other members of the $[\text{Re}_6\text{Q}_8\text{L}_4\text{X}_2]$ ($\text{Q}=\text{S}$ or Se ; $\text{X}=\text{Cl}$ or Br ; $\text{L} = 4,4'$ -bipyridine, 4-phenylpyridine) cluster family have a similar electronic structure to $[\text{Re}_6\text{S}_8\text{bipy}_4\text{Cl}_2]$, tendencies made in the current work can most likely also be applied to these compounds.

Supplementary Materials: The following supporting information can be downloaded at: <https://www.mdpi.com/article/10.3390/molecules28093658/s1>, Optimized coordinates of the $[\text{Re}_6\text{S}_8\text{Cl}_2\text{bipy}_4]^n$ clusters (Tables S1–S9), The bonding and antibonding hypothetical MOs in bipy_4 fragment (Figure S1), ELF slice plane for $\text{Re}_6\text{S}_8\text{bipy}_4\text{Cl}_2$ cluster (Figure S2) and The average QTAIM charges for $[\text{Re}_6\text{S}_8\text{bipy}_4\text{Cl}_2]^n$ ($n = 0, 2-, 4-, 6-, 8-$) cluster (Table S10).

Author Contributions: Data curation, Formal analysis, Resources, Writing—review and editing, M.R.R. and Y.M.G.; Writing—original draft, M.R.R., A.A.U. and Y.M.G.; Funding acquisition, S.G.K. and Y.V.M.; Investigation, Methodology, Visualization, M.R.R. and D.O.A.; Supervision, S.G.K., Y.V.M. and Y.M.G. All authors have read and agreed to the published version of the manuscript.

Funding: The authors acknowledge the Ministry of Science and Higher Education of the Russian Federation (projects 121031700313-8, 121031700321-3).

Institutional Review Board Statement: Not applicable.

Informed Consent Statement: Not applicable.

Data Availability Statement: The data that support the findings of this study are available from the corresponding author upon reasonable request.

Conflicts of Interest: The authors declare no conflict of interest.

Sample Availability: No.

References

1. Shul'pin, G.B.; Kozlov, Y.N.; Shul'pina, L.S. Metal Complexes Containing Redox-Active Ligands in Oxidation of Hydrocarbons and Alcohols: A Review. *Catalysts* **2019**, *9*, 1046. [CrossRef]
2. Pardo, E.; Ruiz-García, R.; Cano, J.; Ottenwaelder, X.; Lescouëzec, R.; Journaux, Y.; Lloret, F.; Julve, M. Ligand design for multidimensional magnetic materials: A metallocsupramolecular perspective. *Dalton Trans.* **2008**, *21*, 2780–2805. [CrossRef]
3. Ma, X.; Suturina, E.A.; Rouzières, M.; Platunov, M.; Wilhelm, F.; Rogalev, A.; Clérac, R.; Dechambenoit, P. Using Redox-Active π Bridging Ligand as a Control Switch of Intramolecular Magnetic Interactions. *J. Am. Chem. Soc.* **2019**, *141*, 7721–7725. [CrossRef] [PubMed]
4. Lyaskovskyy, V.; de Bruin, B. Redox Non-Innocent Ligands: Versatile New Tools to Control Catalytic Reactions. *ACS Catal.* **2012**, *2*, 270–279. [CrossRef]
5. Cameron, J.M.; Holc, C.; Kibler, A.J.; Peake, C.L.; Walsh, D.A.; Newton, G.N.; Johnson, L.R. Molecular redox species for next-generation batteries. *Chem. Soc. Rev.* **2021**, *50*, 5863–5883. [CrossRef]
6. Du, H.-Y.; Chen, S.-C.; Su, X.-J.; Jiao, L.; Zhang, M.-T. Redox-Active Ligand Assisted Multielectron Catalysis: A Case of CoIII Complex as Water Oxidation Catalyst. *J. Am. Chem. Soc.* **2018**, *140*, 1557–1565. [CrossRef]
7. Balzani, V.; Juris, A.; Venturi, M.; Campagna, S.; Serroni, S. Luminescent and Redox-Active Polynuclear Transition Metal Complexes. *Chem. Rev.* **1996**, *96*, 759–834. [CrossRef]
8. Crabtree, R.H. Multifunctional ligands in transition metal catalysis. *New J. Chem.* **2011**, *35*, 18–23. [CrossRef]
9. Kaim, W. Manifestations of Noninnocent Ligand Behavior. *Inorg. Chem.* **2011**, *50*, 9752–9765. [CrossRef]
10. Gray, T.G.; Rudzinski, C.M.; Meyer, E.E.; Holm, R.H.; Nocera, D.G. Spectroscopic and Photophysical Properties of Hexanuclear Rhenium(III) Chalcogenide Clusters. *J. Am. Chem. Soc.* **2003**, *125*, 4755–4770. [CrossRef]
11. Fedorov, V.E.; Yu, V.M.; Naumov, N.G.; Sokolov, M.N.; Vladimir, P.F. Chalcogenide clusters of Group 5–7 metals. *Russ. Chem. Rev.* **2007**, *76*, 529. [CrossRef]
12. Naumov, N.G.; Virovets, A.V.; Fedorov, V.E. Octahedral rhenium(III) chalcocyanide cluster anions: Synthesis, structure, and solid state design. *J. Struct. Chem.* **2000**, *41*, 499–520. [CrossRef]
13. Gabriel, J.-C.P.; Boubekour, K.; Uriel, S.; Batail, P. Chemistry of Hexanuclear Rhenium Chalcogenide Clusters. *Chem. Rev.* **2001**, *101*, 2037–2066. [CrossRef] [PubMed]
14. Perrin, A.; Perrin, C. The molybdenum and rhenium octahedral cluster chalcogenides in solid state chemistry: From condensed to discrete cluster units. *Comptes Rendus Chim.* **2012**, *15*, 815–836. [CrossRef]
15. Pinkard, A.; Champsaur, A.M.; Roy, X. Molecular Clusters: Nanoscale Building Blocks for Solid-State Materials. *Acc. Chem. Res.* **2018**, *51*, 919–929. [CrossRef]
16. Yoshimura, T.; Umakoshi, K.; Sasaki, Y.; Sykes, A.G. Synthesis, Structures, and Redox Properties of Octa(μ_3 -sulfido)hexarhenium(III) Complexes Having Terminal Pyridine Ligands. *Inorg. Chem.* **1999**, *38*, 5557–5564. [CrossRef]
17. Yoshimura, T.; Umakoshi, K.; Sasaki, Y.; Ishizaka, S.; Kim, H.-B.; Kitamura, N. Emission and Metal- and Ligand-Centered-Redox Characteristics of the Hexarhenium(III) Clusters trans- and cis-[Re₆(μ_3 -S)₈Cl₄(L)₂]₂-, Where L Is a Pyridine Derivative or Pyrazine. *Inorg. Chem.* **2000**, *39*, 1765–1772. [CrossRef] [PubMed]
18. Yoshimura, T.; Suo, C.; Tsuge, K.; Ishizaka, S.; Nozaki, K.; Sasaki, Y.; Kitamura, N.; Shinohara, A. Excited-State Properties of Octahedral Hexarhenium(III) Complexes with Redox-active N-heteroaromatic Ligands. *Inorg. Chem.* **2010**, *49*, 531–540. [CrossRef]
19. Yoshimura, T.; Nishizawa, H.; Nagata, K.; Ito, A.; Sakuda, E.; Ishizaka, S.; Kitamura, N.; Shinohara, A. Tuning the Ground- and Excited-State Redox Potentials of Octahedral Hexanuclear Rhenium(III) Complexes by the Combination of Terminal Halide and N-Heteroaromatic Ligands. *ACS Omega* **2022**, *7*, 26965–26982. [CrossRef]
20. Saito, T.; Yoshikawa, A.; Yamagata, T.; Imoto, H.; Unoura, K. Synthesis, structure and electronic properties of octakis(μ_3 -sulfido)hexakis(triethylphosphine)hexatungsten as a tungsten analog of the molecular model for superconducting Chevrel phases. *Inorg. Chem.* **1989**, *28*, 3588–3592. [CrossRef]
21. Chen, Z.-N.; Yoshimura, T.; Abe, M.; Sasaki, Y.; Ishizaka, S.; Kim, H.-B.; Kitamura, N. Chelate Formation around a Hexarhenium Cluster Core by the Diphosphane Ligand Ph₂P(CH₂)₆PPh₂. *Angew. Chem. Int. Ed.* **2001**, *40*, 239–242. [CrossRef]
22. Chen, Z.-N.; Yoshimura, T.; Abe, M.; Tsuge, K.; Sasaki, Y.; Ishizaka, S.; Kim, H.-B.; Kitamura, N. Octa(μ_3 -selenido)hexarhenium(III) Complexes Containing Axial Monodentate Diphosphine or Diphosphine–Monoxide Ligands. *Chem.–A Eur. J.* **2001**, *7*, 4447–4455. [CrossRef]
23. Sokolov, M.N.; Brylev, K.A.; Abramov, P.A.; Gallyamov, M.R.; Novozhilov, I.N.; Kitamura, N.; Mikhaylov, M.A. Complexes of {W₆I₈}₄₊ Clusters with Carboxylates: Preparation, Electrochemistry, and Luminescence. *Eur. J. Inorg. Chem.* **2017**, *2017*, 4131–4137. [CrossRef]

24. Kirakci, K.; Kubát, P.; Langmaier, J.; Polívka, T.; Fuciman, M.; Fejfarová, K.; Lang, K. A comparative study of the redox and excited state properties of (nBu₄N)₂[Mo₆X₁₄] and (nBu₄N)₂[Mo₆X₈(CF₃COO)₆] (X = Cl, Br, or I). *Dalton Trans.* **2013**, *42*, 7224–7232. [[CrossRef](#)]
25. Mikhailov, M.A.; Brylev, K.A.; Abramov, P.A.; Sakuda, E.; Akagi, S.; Ito, A.; Kitamura, N.; Sokolov, M.N. Synthetic Tuning of Redox, Spectroscopic, and Photophysical Properties of [Mo₆I₈]⁴⁺ Core Cluster Complexes by Terminal Carboxylate Ligands. *Inorg. Chem.* **2016**, *55*, 8437–8445. [[CrossRef](#)]
26. Akagi, S.; Fujii, S.; Horiguchi, T.; Kitamura, N. pK_a(L) Dependences of Structural, Electrochemical, and Photophysical Properties of Octahedral Hexamolybdenum(II) Clusters: [Mo₆X₈L₆]^{2−} (X = Br or I; L = carboxylate). *J. Clust. Sci.* **2017**, *28*, 757–772. [[CrossRef](#)]
27. Gushchin, A.L.; Laricheva, Y.A.; Sokolov, M.N.; Llusar, R. Tri- and tetranuclear molybdenum and tungsten chalcogenide clusters: On the way to new materials and catalysts. *Russ. Chem. Rev.* **2018**, *87*, 670. [[CrossRef](#)]
28. Gushchin, A.L.; Laricheva, Y.A.; Abramov, P.A.; Virovets, A.V.; Vicent, C.; Sokolov, M.N.; Llusar, R. Homoleptic Molybdenum Cluster Sulfides Functionalized with Noninnocent Diimine Ligands: Synthesis, Structure, and Redox Behavior. *Eur. J. Inorg. Chem.* **2014**, *2014*, 4093–4100. [[CrossRef](#)]
29. Gushchin, A.L.; Sokolov, M.N.; Peresypkina, E.V.; Virovets, A.V.; Kozlova, S.G.; Zakharchuk, N.F.; Fedin, V.P. Crystal Structure, Electronic Structure, and Solid-State Electrochemistry of Cluster Complexes of M₃Se₇⁴⁺ (M = Mo, W) with Noninnocent o-Phenanthroline and Se₂^{2−} Ligands. *Eur. J. Inorg. Chem.* **2008**, *2008*, 3964–3969. [[CrossRef](#)]
30. Ulantikov, A.A.; Gayfulin, Y.M.; Ivanov, A.A.; Sukhikh, T.S.; Ryzhikov, M.R.; Brylev, K.A.; Smolentsev, A.I.; Shestopalov, M.A.; Mironov, Y.V. Soluble Molecular Rhenium Cluster Complexes Exhibiting Multistage Terminal Ligands Reduction. *Inorg. Chem.* **2020**, *59*, 6460–6470. [[CrossRef](#)]
31. Ulantikov, A.A.; Gayfulin, Y.M.; Sukhikh, T.S.; Ryadun, A.A.; Ryzhikov, M.R.; Mironov, Y.V. Synthesis, Structure, and Physicochemical Properties of Molecular Rhenium Cluster Complexes with 4-Phenylpyridine Molecules as Terminal Ligands. *J. Struct. Chem.* **2021**, *62*, 1009–1019. [[CrossRef](#)]
32. Ulantikov, A.A.; Sukhikh, T.S.; Gribov, E.N.; Maltseva, N.V.; Brylev, K.A.; Mironov, Y.V.; Gayfulin, Y.M. Thermally Controlled Synthesis of Octahedral Rhenium Clusters with 4,4′-Bipyridine and CN[−] Apical Ligands. *Symmetry* **2021**, *13*, 2187. [[CrossRef](#)]
33. Ulantikov, A.A.; Brylev, K.A.; Sukhikh, T.S.; Mironov, Y.V.; Muravieva, V.K.; Gayfulin, Y.M. Octahedral Rhenium Cluster Complexes with 1,2-Bis(4-pyridyl)ethylene and 1,3-Bis(4-pyridyl)propane as Apical Ligands. *Molecules* **2022**, *27*, 7874. [[CrossRef](#)] [[PubMed](#)]
34. ADF2017, SCM, Theoretical Chemistry, Vrije Universiteit, Amsterdam, The Netherlands. Available online: <https://www.scm.com> (accessed on 30 March 2023).
35. te Velde, G.; Bickelhaupt, F.M.; Baerends, E.J.; Fonseca Guerra, C.; van Gisbergen, S.J.A.; Snijders, J.G.; Ziegler, T. Chemistry with ADF. *J. Comput. Chem.* **2001**, *22*, 931–967. [[CrossRef](#)]
36. Swart, M. A new family of hybrid density functionals. *Chem. Phys. Lett.* **2013**, *580*, 166–171. [[CrossRef](#)]
37. Van Lenthe, E.; Baerends, E.J. Optimized Slater-type basis sets for the elements 1–118. *J. Comput. Chem.* **2003**, *24*, 1142–1156. [[CrossRef](#)] [[PubMed](#)]
38. Lenthe, E.V.; Ehlers, A.; Baerends, E.-J. Geometry optimizations in the zero order regular approximation for relativistic effects. *J. Chem. Phys.* **1999**, *110*, 8943–8953. [[CrossRef](#)]
39. Pye, C.C.; Ziegler, T. An implementation of the conductor-like screening model of solvation within the Amsterdam density functional package. *Theor. Chem. Acc.* **1999**, *101*, 396–408. [[CrossRef](#)]
40. Gayfulin, Y.M.; Brylev, K.A.; Ryzhikov, M.R.; Samsonenko, D.G.; Kitamura, N.; Mironov, Y.V. Luminescent twelve-nuclear rhenium clusters. *Dalton Trans.* **2019**, *48*, 12522–12530. [[CrossRef](#)]
41. Artem'ev, A.V.; Ryzhikov, M.R.; Berezin, A.S.; Kolesnikov, I.E.; Samsonenko, D.G.; Bagryanskaya, I.Y. Photoluminescence of Ag(I) complexes with a square-planar coordination geometry: The first observation. *Inorg. Chem. Front.* **2019**, *6*, 2855–2864. [[CrossRef](#)]
42. Yarovoy, S.S.; Ivanova, M.; Sukhikh, T.S.; Ryzhikov, M.R.; Fedorov, V.E.; Naumov, N.G. Replenishment in the Family of Rhenium Chalcobromides; Synthesis and Structure of Molecular {Re₄S₄}Br₈(TeBr₂)₄, Dimeric [{Re₄S₄}Br₈(TeBr₂)₃]₂, and Polymeric {Re₄S₄}Br₈ Compounds Based on the {Re₄S₄}⁸⁺ Tetrahedral Cluster Core. *Inorg. Chem.* **2022**, *61*, 20472–20479. [[CrossRef](#)]
43. Baranov, A.Y.; Rakhmanova, M.I.; Hei, X.; Samsonenko, D.G.; Stass, D.V.; Bagryanskaya, I.Y.; Ryzhikov, M.R.; Fedin, V.P.; Li, J.; Artemev, A.V. A new subclass of copper(I) hybrid emitters showing TADF with near-unity quantum yields and a strong solvatochromic effect. *Chem. Commun.* **2023**, *59*, 2923–2926. [[CrossRef](#)] [[PubMed](#)]
44. Becke, A.D.; Edgecombe, K.E. A simple measure of electron localization in atomic and molecular systems. *J. Chem. Phys.* **1990**, *92*, 5397–5403. [[CrossRef](#)]
45. Silvi, B.; Savin, A. Classification of chemical bonds based on topological analysis of electron localization functions. *Nature* **1994**, *371*, 683–686. [[CrossRef](#)]
46. Kohout, M. *DGrid*; Version 4.6; SitePen: Radebeul, Germany, 2011.
47. Bader, R.F.W. *Atoms in Molecules: A Quantum Theory*; Clarendon Press: Oxford, UK, 1990.
48. Bickelhaupt, F.M.; Baerends, E.J. Kohn-Sham Density Functional Theory: Predicting and Understanding Chemistry. In *Reviews in Computational Chemistry*; Wiley-VCH: New York, NY, USA, 2000; pp. 1–86. [[CrossRef](#)]
49. ADF 2020, SCM, Theoretical Chemistry, Vrije Universiteit, Amsterdam, The Netherlands. Available online: <https://www.scm.com> (accessed on 30 March 2023).

50. Ryzhikov, M.R.; Kozlova, S.G. Reduction of carbon and nitrogen centered trigonal prismatic tungsten clusters: Bonding patterns as viewed by ELF and AIM methods. *Polyhedron* **2019**, *173*, 114131. [[CrossRef](#)]
51. Kryuchkova, N.A.; Ryzhikov, M.R.; Syrovashin, M.M. Interatomic Interactions in Heterometallic Cubane-Type Clusters with {Mo₃S₄M'} (M' = Cu, Ni, Pd) Core. *J. Clust. Sci.* **2021**, *32*, 415–421. [[CrossRef](#)]
52. Michalski, M.; Berski, S. Exploring the Relationship between Reactivity and Electronic Structure in Isorhodanine Derivatives Using Computer Simulations. *Molecules* **2023**, *28*, 2360. [[CrossRef](#)]
53. Kégl, T.R.; Pálkás, N.; Kollár, L.; Kégl, T. Computational Characterization of Bidentate P-Donor Ligands: Direct Comparison to Tolman's Electronic Parameters. *Molecules* **2018**, *23*, 3176. [[CrossRef](#)] [[PubMed](#)]

Disclaimer/Publisher's Note: The statements, opinions and data contained in all publications are solely those of the individual author(s) and contributor(s) and not of MDPI and/or the editor(s). MDPI and/or the editor(s) disclaim responsibility for any injury to people or property resulting from any ideas, methods, instructions or products referred to in the content.